

Photoemission from Ir(001): Evidence for an Orbital Angular Momentum Dependence to X-Ray Photoelectron Diffraction

L. E. Klebanoff^(a) and D. G. Van Campen^(b)

Department of Chemistry and Zettlemoyer Center for Surface Studies, Lehigh University, Bethlehem, Pennsylvania 18015

(Received 16 August 1991)

Polar angle x-ray photoelectron diffraction (XPD) curves are presented for the Ir(001) $5p_{3/2}$, $4f_{7/2}$, $4d_{5/2}$, $4p_{3/2}$, and $4s_{1/2}$ core levels, as well as for the valence band. The core-level XPD intensity enhancements along the [001] and [011] crystallographic directions show a substantial dependence on the initial-state orbital angular momentum l_i . XPD from regions within the Ir valence band correlate well with core-level XPD of the same l_i . This correlation indicates that l_i -dependent XPD can influence the angular dependence of spectral intensities within angle-resolved x-ray photoemission valence-band spectra.

PACS numbers: 79.60.Cn, 61.14.Rq, 68.35.Bs

X-ray photoelectron diffraction (XPD) is the name given to a class of angle-dependent intensity variations in angle-resolved x-ray photoelectron spectroscopy (XPS) [1]. The phenomenon is due to the interference between the directly propagating unscattered wave and the elastically scattered wave in the photoemission final state. The sensitivity of the technique to crystalline geometry has made XPD a powerful probe of solid-state geometric structure [1].

Our studies are motivated by recent advances [2,3] in the theoretical modeling of XPD data that have predicted a dependence of the amplitude of the XPD on the orbital angular momentum involved in the dipole photoelectric excitation. We present here a comparison of the polar-angle-dependent XPD for the Ir(001) $5p_{3/2}$, $4f_{7/2}$, $4d_{5/2}$, $4p_{3/2}$, and $4s_{1/2}$ core levels, as well as for the valence band. The results show a significant dependence of diffraction intensity on the initial state that can most consistently be described as a dependence of XPD on orbital angular momentum.

The experiments were conducted using Lehigh University's SCIENTA ESCA-300 x-ray photoelectron spectrometer, employing an angular acceptance of $\pm 1.7^\circ$, a photon energy of 1486.6 eV, and an instrumental energy resolution of 0.82 eV FWHM. The spectrometer provides an exceedingly high sensitivity, stability, and a very flat polar-angle response function, which allows a quantitative comparison of spectral intensities over the angular range of the experiment. Experimental angles are accurate to within 1° . The sample temperature was 298 K for all measurements. Electron kinetic energies (relative to the Fermi level) for the $5p_{3/2}$, $4f_{7/2}$, $4d_{5/2}$, $4p_{3/2}$, and $4s_{1/2}$ core levels are 1438.7, 1426.1, 1190.6, 992.1, and 795.3 eV, respectively.

Our sample was a high-purity Ir(001) single crystal. The crystal was oriented with the Laue method and cleaned *in situ* by argon-ion sputtering and cycles of heating in oxygen (1×10^{-6} Torr) for 5 min at 1200 K. This produced a clean (5×1) reconstructed surface [4] as observed by LEED. However, in the residual vacuum of the preparation chamber (5×10^{-9} Torr) this surface

quickly converted to a $c(2 \times 2)$ structure characteristic of 0.5 monolayer contamination. Carbon and oxygen were the only contaminants, as determined by XPS. While not aesthetically pleasing, this half monolayer of contaminants produced a surface that was devoid of the complicating effects of the Ir(001) surface reconstruction, and stable in the spectrometer vacuum (2×10^{-10} Torr) for days. The carbon $1s$ overlayer photoelectric signal also provided a valuable internal confirmation of the flatness of the instrumental polar-angle response function. The ~ 13 – 20 -Å depth sensitivity of the present measurements [5], as well as previous observations [6], suggest that the surface contamination produces negligible effects on the Ir core-level and valence-band XPD signals.

The Ir core-level and valence-band spectral intensities were measured as a function of the polar angle θ_e between the detector and the [001] surface normal in the (100) mirror plane perpendicular to the [100] direction. For each initial-state XPS spectrum at each θ_e , the inelastic spectral background was fitted with a Shirley background [7] and the integrated area above this background was recorded. These integrated spectral intensities $I(\theta_e)$ were measured at 2° intervals in the range -10° to 56° by rotating the sample. The $\theta_e = 0^\circ$ direction corresponds to [001]; $\theta_e = 45^\circ$ corresponds to [011].

The XPD data are presented in the traditional "chi" form: $\chi(\theta_e) = [I(\theta_e) - I_0]/I_0$. Theoretically, I_0 is the spectral intensity in the absence of diffraction effects. Such I_0 values were generated by measuring core-level and valence-band XPS intensities from clean polycrystalline Ir. These relative polycrystalline I_0 values match to within 3% or less the relative I_0 values obtained by angle averaging the Ir(001) XPS data, the small discrepancy being due to the fact that an angle average over $\sim 66^\circ$ is not sufficient to completely remove XPD effects. The polycrystalline Ir measurements provide the conceptually correct and slightly more accurate relative I_0 values needed to compare the $\chi(\theta_e)$ curves for different initial states. All of the XPD data, except for the $4s_{1/2}$ level [8], employ I_0 values in relative agreement with the polycrystalline Ir measurements. The reproducibility of our intensi-

ty data is poorest for the very weak $4s_{1/2}$ level. For this level the intensity reproducibility was $\sim 5\%$.

Figure 1 compares $\chi(\theta_e)$ versus the polar angle θ_e for the $4s_{1/2}(l_i=0, l_f=1)$, $5p_{3/2}(l_i=1, l_f=0,2)$, $4d_{5/2}(l_i=2, l_f=1,3)$, and $4f_{7/2}(l_i=3, l_f=2,4)$ core levels of Ir(001). Here l_i is the initial-state orbital angular momentum, and l_f is the final-state orbital angular momentum. Peaks at 0° and 45° are due to "zeroth-order" diffraction (i.e., forward scattering) along the [001] and [011] directions, respectively, in the fcc lattice of Ir. The peak at $\theta_e=18^\circ$ coincides with the [013] direction and may represent forward scattering through atoms along [013]. However, the peaks at $\theta_e=18^\circ$ and 32° are likely to have a strong contribution from first-order diffraction associated with scattering from atoms along the [001] and [011] directions. Our discussion will focus entirely on the forward scattering intensity enhancements at $\theta_e=0^\circ$ and $\theta_e=45^\circ$ that have a clear origin.

Figure 1 shows that the intensity enhancement $\chi(\theta_e)$ produced by forward scattering is dependent on the core-level initial state, and that this dependence is itself a function of the geometry of the scattering. For emission

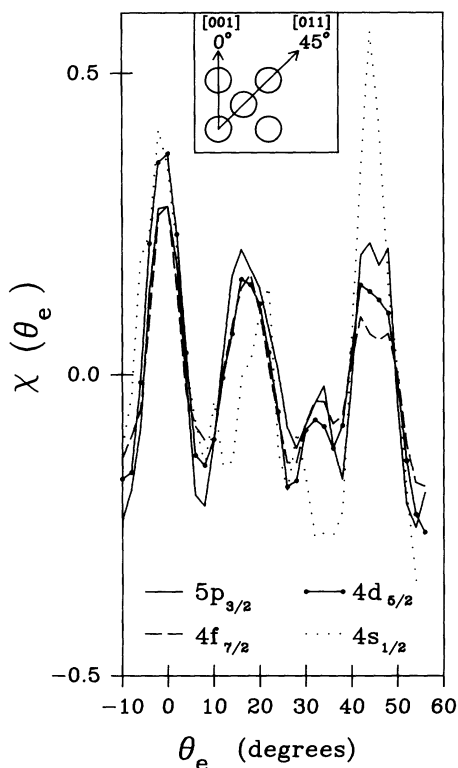


FIG. 1. Polar-angle XPD from Ir(001) for various core levels. $\chi(\theta_e)$ is defined in the text. The angle θ_e indicates the polar angle of photoelectron detection. Inset: The relationship between θ_e and Ir atomic positions in the (100) mirror plane. $\theta_e=0^\circ$ corresponds to the [001] crystallographic direction; $\theta_e=45^\circ$ corresponds to the [011] direction. Graph lines connect experimental data points.

along $\theta_e=0^\circ$, the $4d_{5/2}$ and $4s_{1/2}$ levels show the strongest enhancement, followed by the $5p_{3/2}$ and $4f_{7/2}$ levels. For emission along $\theta_e=45^\circ$, the order of the intensity enhancement changes significantly. The $4s_{1/2}$ level shows a very strong enhancement, followed in order by the $5p_{3/2}$, $4d_{5/2}$, and $4f_{7/2}$ levels. A striking aspect of Fig. 1 is that the ratio of the enhancement along [011] ($\theta_e=45^\circ$) to that along [001] ($\theta_e=0^\circ$) decreases significantly as l_i increases.

The Ir $4f_{7/2}$ and $4f_{5/2}$ levels produced identical $\chi(\theta_e)$ curves, as did the $4d_{5/2}$ and $4d_{3/2}$ levels. This suggests that initial states with the same l_i , but small differences in binding energy, produce the same XPD curves, with no detectable dependence on the spin-orbit interaction.

Figure 2 indicates that the form of XPD curves for the zeroth-order scattering along [001] and [011] is very similar for initial states with the same l_i , even with large differences in binding energy. Both the $\chi(0^\circ)$ and $\chi(45^\circ)$ enhancements are very similar for the $4p_{3/2}$ and $5p_{3/2}$ levels, even though their binding energies differ by 446.6 eV. Also, the ratio of the enhancement along [011] to that along [001] is identical for the $4p_{3/2}$ and $5p_{3/2}$ core levels.

One cannot consistently relate the core-level XPD data in Figs. 1 and 2 to the different electron kinetic energies (or the different escape depths) of the core-level photoelectrons. The $5p_{3/2}$ and $4p_{3/2}$ peaks (both $l_i=1$) show good agreement for $\chi(0^\circ)$ and $\chi(45^\circ)$ despite the 446.6-eV kinetic energy difference, while the $4f_{7/2}(l_i=3)$ and $5p_{3/2}(l_i=1)$ levels show significant differences despite being separated by only 12.6 eV in kinetic energy. In addition, the identical curves generated from the $4f$ and $4d$ spin-orbit split components indicate that when two initial

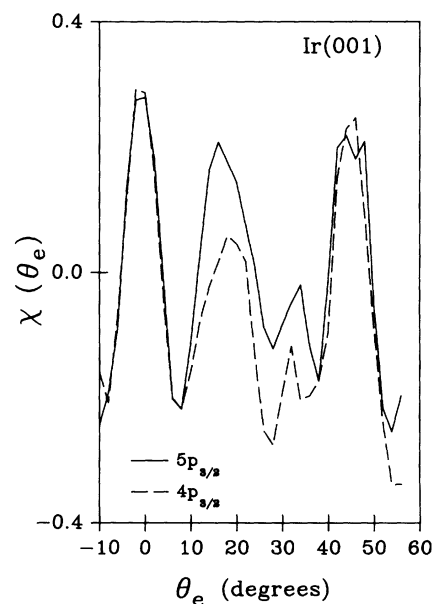


FIG. 2. Comparison of polar-angle XPD for the Ir $5p_{3/2}$ and $4p_{3/2}$ core levels. Graph lines connect experimental data points.

states have the same l_i , then identical $\chi(\theta_e)$ curves can result even with small differences in kinetic energy.

Thus, the *differences* observed in Fig. 1 between the various initial states with *different* l_i and the *similarities* observed in Fig. 2 between two different initial states with *the same* l_i , are most consistently explained as a dependence of XPD on the initial-state orbital angular momentum l_i .

No theoretical results exist for XPD from Ir. We can, however, qualitatively compare our experimental results with the single-scattering spherical-wave theoretical work of Friedman and Fadley [2]. Their calculations modeled the dependence of XPD on l_i for a photoemitting Cu atom located 3.5 Å away from a single Cu scatterer. Their results for the high kinetic energy of 1000 eV can be summarized as follows [2]: Increasing the initial-state orbital angular momentum from $l_i=0$ to $l_i=3$ systematically decreases the amplitude of the forward scattering intensity $\chi(\theta_e)$. An additional more subtle effect of increasing l_i is the "filling in" of the first minimum of $\chi(\theta_e)$ between the zeroth-order diffraction peak and the first-order diffraction peak.

Our XPD results are in qualitative agreement with the theory of Friedman and Fadley in that an l_i dependence is observed. However, the differences observed in Fig. 1 for the [001] [$\chi(0^\circ)$] and [011] [$\chi(45^\circ)$] directions show that the ordering of the enhancements for the different l_i depends on the scattering geometry—an aspect that has not been examined theoretically. There is evidence in Fig. 1 for the filling-in phenomenon predicted theoretically in the valleys between the zeroth-order and first-order diffraction features.

The l_i dependence in Fig. 1 may be due in part to an l_i dependence of the multiple-scattering "defocusing" that is known to occur [9] for electron propagation along chains of atoms. This could explain why the differences in the $\chi(\theta_e)$ are greater for the high atomic density [011] direction than for the less dense [001] direction.

It is natural to speculate that Ir *valence-band* initial states retain a sufficiently well-defined orbital angular momentum character to display XPD effects analogous to XPD from core levels with the same l_i . Figure 3(a) displays a normal emission ($\theta_e=0^\circ$) valence-band XPS spectrum for Ir(001). The dashed line represents the Shirley inelastic background estimated for this spectrum. We divide the valence-band spectrum into two regions. Region 1 covers the binding energy region 14.0 to 5.5 eV. From band structure calculations [10] one expects the spectral intensity in region 1 to have $\sim 90\%$ $6s$ character, $\sim 10\%$ $6p$ character, and virtually zero $5d$ character. Region 2 covers the binding energy range 4.25 to -2.0 eV. Band theory [10] and cross-section considerations [11] indicate that the spectral intensity of region 2 should be almost entirely $5d$ in character. The integrated spectral intensities above the inelastic background in these two regions were measured as a function of the polar angle θ_e in

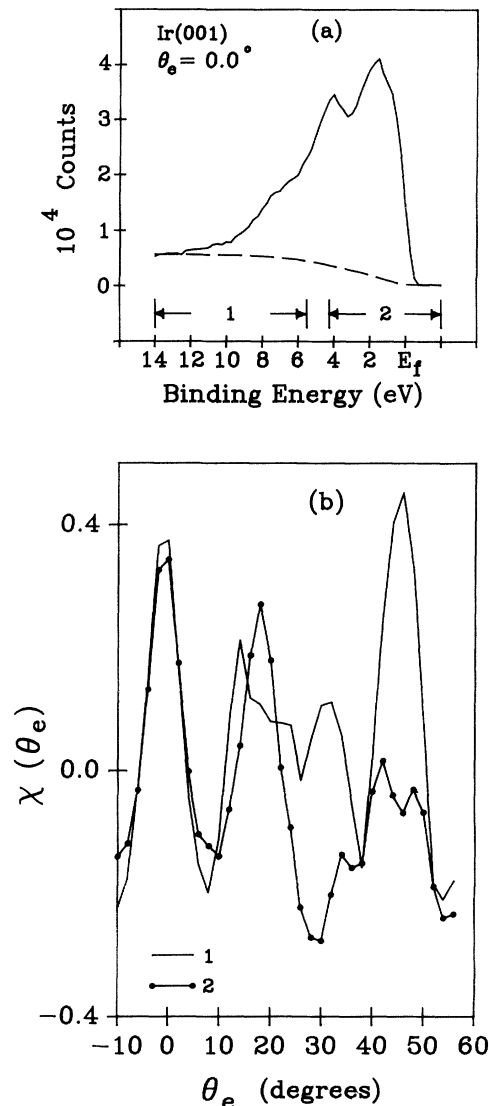


FIG. 3. (a) Valence-band XPS spectrum from Ir(001). Region 1 covers 14.0 to 5.5 eV binding energy. Region 2 covers 4.5 to -2 eV binding energy. The Fermi level is 0.0 eV binding energy. (b) Comparison of polar-angle XPD for the valence regions 1 and 2. Graph lines connect experimental data points.

the same manner as the core-level measurements of Figs. 1 and 2. The results are shown in Fig. 3(b).

Both regions 1 and 2 show strong diffraction effects. This is not too surprising, since energy-integrated valence-band XPD has been observed in Au [12], Al [13], and W [1]. However, regions 1 and 2 display $\chi(\theta_e)$ curves quite different from each other, yet very similar to XPD from core levels of the same l_i . Region 1 ($6s$ character with a small contribution from $6p$ states) shows $\chi(0^\circ)$ and $\chi(45^\circ)$ enhancements in good agreement with the $4s_{1/2}$ core-level XPD data of Fig. 1, particularly with regard to the amplitude and angular width of the XPD

enhancement. Region 2 ($5d$ character) shows a strong $\chi(0^\circ)$ and a weak $\chi(45^\circ)$ in qualitative agreement with the $4d_{5/2}$ core-level XPD data. The similarity between the XPD data from a core level of given l_i and the XPD data from a valence-band region with the same l_i strongly suggests that *the angle-dependent XPD from a valence-band state in Ir can to a large extent be determined by that state's orbital angular momentum l_i .*

One might suspect that some of the intensity variations in Fig. 3 could be due to direct photoelectric transitions. Ir has a rather large Debye-Waller factor of 0.60, suggesting that direct (wave-vector-conserving) transitions could comprise 60% of the valence XPS intensity [14]. However, XPS work on tungsten (with a Debye-Waller factor of 0.55) indicates that "pure" direct transitions contribute only $\sim 25\%$ of the total valence-band XPS intensity, with the remaining 75% attributable to nondirect (wave-vector-integrating) transitions [15]. It should be noted that *energy-integrated* W valence-band XPD differs from W $4f$ core-level data by only $\sim 10\%$ [1], suggesting that direct transitions play a minority role in determining energy-integrated valence-band XPS intensity variations with θ_e .

The same situation is likely true for Ir. Indeed, high energy resolution and high angular resolution XPS studies of the Ir valence band [16] indicate a much smaller direct transition component than that suggested by the Debye-Waller factor. The overall correlation at $\theta_e = 0^\circ$ and 45° between region 1 and the $4s_{1/2}$ core level, and region 2 and the $4d_{5/2}$ core level suggests that l_i -dependent XPD is a major contributor to relative angle-resolved XPS intensity variations within the valence band of Ir.

In summary, XPD from Ir core levels and valence-band states show a substantial dependence on the orbital angular momentum of the initial state l_i . This dependence is found to be particularly strong along the high atomic density [011] direction. Future XPD experiment and theory, both for Ir along different directions and for different elements, will reveal the generality of the observed phenomena.

Financial support for this work came from the Camille and Henry Dreyfus Foundation, the Charles A. Dana Foundation, and Lehigh University. Acknowledgment is also made to the donors of the Petroleum Research Fund, administered by the American Chemical Society, for par-

tial support of the research. The authors thank R. H. Victora and A. C. Miller for helpful discussions.

Note added.—Additional valence-band XPD work on W has been recently reported by Herman *et al.* [17].

(a) Author to whom correspondence should be addressed.

(b) Also at Department of Physics.

- [1] For a review, see C. S. Fadley, in *X-Ray and Inner-Shell Processes*, edited by T. Carlson, M. O. Krause, and S. T. Manson, AIP Conf. Proc. No. 215 (AIP, New York, 1991).
- [2] D. J. Friedman and C. S. Fadley, *J. Electron Spectrosc. Relat. Phenom.* **51**, 689 (1990).
- [3] D. E. Parry, *J. Electron Spectrosc. Relat. Phenom.* **49**, 23 (1989).
- [4] T. N. Rhodin and G. Broden, *Surf. Sci.* **60**, 466 (1976).
- [5] S. Tanuma, C. J. Powell, and D. R. Penn, SIA, *Surf. Interface Anal.* **11**, 577 (1988).
- [6] Cr $2p_{3/2}$ polar-angle XPD plots for clean Cr(001) and $c(2 \times 2)$ N/Cr(001) are identical: L. E. Klebanoff (unpublished).
- [7] D. A. Shirley, *Phys. Rev. B* **5**, 4709 (1972).
- [8] Our polycrystalline Ir sample contained 1% Fe impurity. The Fe $2p_{3/2}$ XPS peak interferes with the Ir $4s_{1/2}$ XPS peak, making an accurate $4s_{1/2}$ intensity measurement difficult. For the Ir(001) $4s_{1/2}$ $\chi(\theta_e)$ curve, we used for I_0 the angle-averaged intensity. We estimate the resulting error in I_0 to be less than 3%.
- [9] M.-L. Xu, J. J. Barton, and M. A. Van Hove, *Phys. Rev. B* **39**, 8275 (1989).
- [10] R. H. Victora (private communication). See also O. K. Andersen, *Phys. Rev. B* **2**, 883 (1970).
- [11] J. H. Scofield, *J. Electron Spectrosc. Relat. Phenom.* **8**, 129 (1976).
- [12] R. J. Baird, C. S. Fadley, and L. F. Wagner, *Phys. Rev. B* **15**, 666 (1977).
- [13] J. Osterwalder, T. Greber, S. Hüfner, and L. Schlapbach, *Phys. Rev. Lett.* **64**, 2683 (1990).
- [14] Z. Hussain, C. S. Fadley, S. Kono, and L. F. Wagner, *Phys. Rev. B* **22**, 3750 (1980).
- [15] R. C. White, C. S. Fadley, M. Sagurton, and Z. Hussain, *Phys. Rev. B* **34**, 5226 (1986).
- [16] L. E. Klebanoff and D. G. Van Campen (to be published).
- [17] G. S. Herman, T. T. Tran, K. Higashiyama, and C. S. Fadley, *Phys. Rev. Lett.* **68**, 1204 (1992).